Numerical simulation of thermal convection in a fluid with the infinite Prandtl number and its application to a glass manufacturing problem

Hajime ITOH

ABSTRACT. Thermal convection phenomena of fluids with the infinite Prandtl number are studied via numerical simulations. These phenomena are governed by various physical mechanisms in a glass melting furnace that affect the quality of glass. As an extension of the numerical model for thermal convection phenomena with the infinite Prandtl number, we present an effective finite element scheme that is called a stabilized method and enables us to carry out stable computation even for the cases of high Rayleigh numbers. By means of this scheme, transient growth of thermal convection in a topcooled rectangular domain is studied. This problem is regarded as a model of cooling process in a glass melting furnace. The computational results reveal the mechanism of generating debasement of glass quality in the cooling process. Applying the results of the simulations, we present a new cooling method that enables us to shorten a residence time that is necessary for cooling without debasement of glass quality.

1. Introduction

In this paper we study transient thermal convection of fluid flows with the infinite Prandtl number by applying numerical simulations. This work is motivated by the study of quality debasement in the glass production in the glass melting furnace. Figure 1(a) shows a schematic illustration of a typical glass melting furnace producing the sheet glass. Figure 1(b) shows cross sectional illustrations of the melting and cooling sections of the furnace. In the glass melting furnace, glass materials are heated up to about 1500° C in the melting section and then molten glass is cooled down to about 1100° C in the cooling section. As shown in Figure 1(b), the molten glass is placed in two different types of thermal conditions in the furnace. In the melting section the temperature of the molten glass is high on the top surface and low at the bottom because it is heated on the top surface and cooled at the bottom


Hajime Iтон
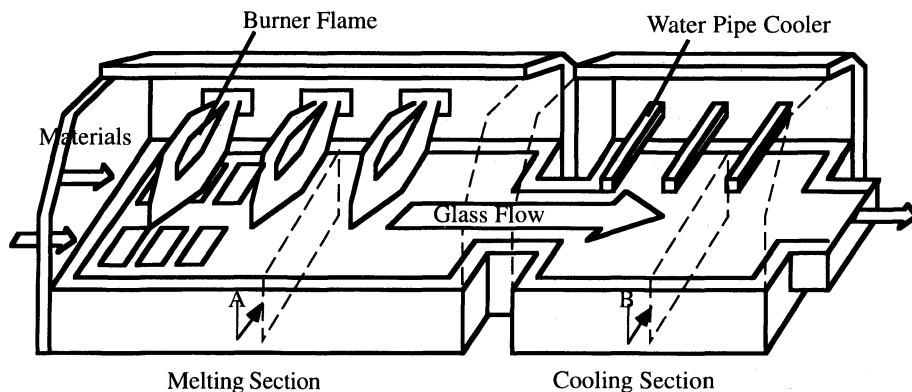
Figure 1(a): Schematic figure of a typical glass melting furnace for the sheet glass.
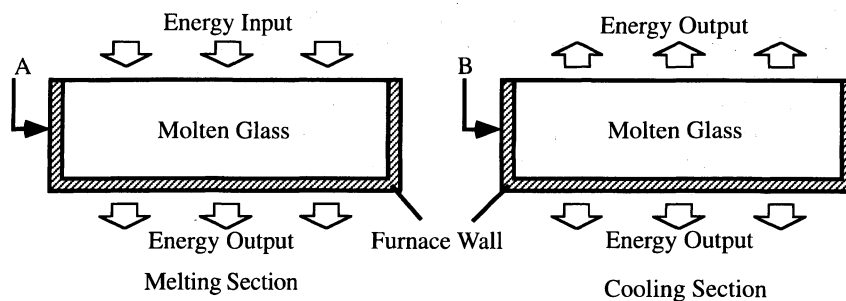
Figure 1(b): Cross sectional figures of the melting section and the cooling section of the furnace.

through the wall of the furnace. On the other hand, in the cooling section, molten glass is cooled on both top and bottom surfaces. Especially in the case of production of dark colored glass, glass manufacturers often suffer from the growth of Rayleigh-Benard cells near the surface in the process of cooling section because of top-cooling, which causes an optical distortion on the glass surface. The purpose of this work is to clarify essential phenomena in the cooling process in glass furnaces and then present a new operation method in the cooling section of glass melting furnaces by means of the numerical approach.

Thermal convection phenomena of fluids with high or infinite Prandtl numbers are typical physical phenomena that appear in the earth mantle as well as in the convection of molten glass in glass furnaces. It is noteworthy that the phenomena in glass melting furnaces is very similar to those in the mantle in the sense of having high or infinite Prandtl numbers. Numerical approaches to the study of the mantle convection have been discussed in [8], [9], [19], [22],

[25] and [26]. These results simulate the internal flows in the mantle, under the condition of fixed cold boundary on the top and hot at the bottom. The Rayleigh number of the mantle convection is of order of 10^6 [19].

Numerical simulations in the process of the glass melting furnaces have been extensively performed to develop effective methods in optimal furnace designing and glass production of higher quality and efficiency in glass manufacturing [11], [12], [18]. Steady [12], [18] or unsteady [11] simulations have been made to describe the phenomena in the furnace, while it seems to the best of the author's knowledge that there is no literature that describes the details of the top-cooled Rayleigh-Benard convection.

The analysis of Rayleigh-Benard problems has been made in various ways. Theoretical approaches to the evaluation of the critical Rayleigh number are considered in [14], [20]. Numerical approaches to the problem are treated in [4], [17], [21]. In these papers the critical Rayleigh number for the bottom heated problem are discussed under the condition that temperature is fixed on the top and bottom boundaries and isothermal initial conditions. However these results are not directly applicable to our problem.

As for numerical computation, an appropriate finite difference method or finite element method is usually used. The detailed mathematical studies of the finite element schemes for thermal convection phenomena are made in [1], [2] in conventional flow problems and problems for the infinite Prandtl number are treated in [13].

As shown in Section 4, the Rayleigh number of the cooling section is of order from 10^5 to 10^6. From this it is seen that some upwind techniques for numerical schemes are necessary. Based on a scheme for the thermal convection problem for the infinite Prandtl number [13], we present a stabilized finite element scheme that makes the computation stable for the case of high Rayleigh numbers. The stabilized schemes we here use for the advection-diffusion problems have been developed in [5], [10]. By means of this scheme, transient growth of thermal convection in a top-cooled rectangular domain is studied. This problem is regarded as a 2-dimensional model of cooling process in a glass melting furnace.

The contents of the paper are organized as follows. In Section 2, basic equations for thermal convection flows with the infinite Prandtl number are formulated. In Section 3, a stabilized finite element scheme for the problem is presented and the error analysis of this scheme is examined via a sample numerical simulation. In Section 4, the transient growth of thermal convection in a top-cooled rectangular domain is studied through numerical simulations. Using such simulations, we present a new cooling method that enables us to shorten a residence time necessary for cooling without quality debasement. In section 5, we give concluding remarks.

In what follows, Ω is a bounded domain in $\boldsymbol{R}^d$ with boundary Γ for $d = 2$ or 3. $I \equiv (0, T)$ is a fixed time interval. The boundary Γ is divided into $\Gamma_1 \neq \varnothing$ and Γ_2 where $\overline{\Gamma_1} \cup \overline{\Gamma_2} = \Gamma$ and $\Gamma_1 \cap \Gamma_2 = \varnothing$. $L^2(\Omega)$ is the space of square-integrable functions in Ω whose inner product and norm are denoted by $(\cdot, \cdot)$ and $\| \cdot \|_{0, \Omega}$, respectively. $L_0^2(\Omega)$ is the space of L^2-functions with mean value zero in Ω. $H^k(\Omega)$ is the Sobolev space consisting of functions whose derivatives of order less than or equal to k lie in $L^2(\Omega)$. The norm and semi-norms are denoted by $\| \cdot \|_{k, \Omega}$ and $| \cdot |_{k, \Omega}$, respectively. $H^{-1}(\Omega)$ denotes the dual space of the Sobolev space $H_0^1(\Omega)$ whose norm is denoted by $\| \cdot \|_{-1, \Omega}$. $L^2(\Gamma)$ is the space of square integrable functions on Γ. The symbol $\langle \cdot, \cdot \rangle$ denotes the duality pairing between $H_0^1(\Omega)$ and $H^{-1}(\Omega)$. ∇ is the gradient operator defined by $\nabla \equiv \left(\dfrac{\partial}{\partial x_1}, \dots, \dfrac{\partial}{\partial x_d} \right)$ and Δ is the Laplace operator defined by $\Delta \equiv \displaystyle\sum_{j=1}^{d} \dfrac{\partial^2}{\partial x_j^2}$.

2. Basic equations for thermal convection phenomena with the infinite Prandtl number

We consider the problem of finding a velocity field u, a pressure field p, and a temperature field θ that satisfy the following equations in $\Omega \times (0, T)$:

$$-2\nabla \otimes D(u) + \nabla p = E\theta, \tag{1}$$

$$\nabla \cdot u = 0, \tag{2}$$

$$\frac{\partial \theta}{\partial t} + \mathrm{Ra}\, u \cdot \nabla \theta = \Delta \theta + f, \tag{3}$$

subject to the initial condition

$$\theta = \theta^0, \qquad \text{at } t = 0, \tag{4}$$

and boundary conditions

$$\theta = 0, \quad u = 0, \qquad \text{on } \Gamma_1, \tag{5}$$

$$\frac{\partial \theta}{\partial n} = \zeta, \quad u \cdot n = 0,$$

$$t^{(k)} \cdot D(u)\, n = 0, \quad k = 1, \dots, d-1, \qquad \text{on } \Gamma_2, \tag{6}$$

where $\nabla \otimes D(v)$ is the stress divergence term defined by

$$[\nabla \otimes D(v)]_i \equiv \sum_{j=1}^{d} \frac{\partial}{\partial x_j} D_{ij}(v), \qquad D_{ij}(v) \equiv \frac{1}{2} \left(\frac{\partial v_i}{\partial x_j} + \frac{\partial v_j}{\partial x_i} \right),$$

and $E \in \mathbf{R}^d$ is a unit vector, $(0, 1)$ or $(0, 0, 1)$. The symbol Ra stands for the Rayleigh number and $f : (0, T) \to H^{-1}(\Omega)$ represents a source term. $\zeta : (0, T) \to L^2(\Gamma_2)$ denotes a heat flux on Γ_2. n is a outward normal vector on Γ_2 and $t^{(k)}$, $k = 1, \dots, d - 1$ is a set of orthonormal vectors tangent to Γ_2. The system of equations (1)–(3) is a model of thermal convection phenomena with the infinite Prandtl number. For the derivation of the conventional Boussinesq equations, we refer to [13].

Considering the essential boundary conditions and the uniqueness of solutions to the problem mentioned above, we introduce the three function spaces below:

$$V \equiv \{v \in (H^1(\Omega))^d; v = 0 \text{ on } \Gamma_1, \quad v \cdot n = 0 \text{ on } \Gamma_2\},$$

$$Q \equiv L_0^2(\Omega),$$

$$\Psi \equiv \{\Psi \in H^1(\Omega); \Psi = 0 \text{ on } \Gamma_1\}.$$

We seek a solution $(u, p, \theta) : (0, T) \to V \times Q \times \Psi$.

3. A stabilized finite element scheme for the thermal convection problem associated with the infinite Prandtl number

In this section, we introduce a stabilized finite element scheme for the system of equations in the previous section. The scheme is also stable for the problems with high Rayleigh numbers that we discuss in the next section.

3.1 A Space-Time Finite Element Scheme

We consider a finite element scheme for the thermal convection problem associated with the infinite Prandtl number. Let $\mathfrak{J}_h$ be a triangulation of $\bar{\Omega}$, where h denotes the maximum diameter of all elements $K \in \mathfrak{J}_h$. Let $V_h \subset V$, $Q_h \subset Q$ and $\Psi_h \subset \Psi$ be finite dimensional subspaces. We consider time intervals $I_n \equiv ((n - 1)\Delta t, n\Delta t)$, where $\Delta t > 0$ is a time increment introduced for the time discretization $n = 1, \dots, N_T \equiv \left[\dfrac{T}{\Delta t}\right]$. By using the above notation, we define space-time finite element subspaces [15], [24] by

$$V_h^* \equiv \{v_h^* : I \to V_h; v_h^*(t) = v_h^n \in V_h, \ \forall t \in I_n\},$$

$$Q_h^* \equiv \{q_h^* : I \to Q_h; q_h^*(t) = q_h^n \in Q_h, \ \forall t \in I_n\},$$

$$\Psi_h^* \equiv \{\psi_h^* : I \to \Psi_h; \psi_h^*(t) = \psi_h^n \in \Psi_h, \ \forall t \in I_n\}.$$

These are subspaces of the space-time finite element spaces that consist of functions constant in each time interval I_n. A finite element scheme for the thermal convection problem associated with the infinite Prandtl number is formulated as a problem to find $(u_h^n, p_h^n, \theta_h^n; n = 0, \ldots, N_T) \subset V_h \times Q_h \times \Psi_h$ such that

$$\int_{I_n} a(u_h^n, v_h) + b(v_h, p_h^n) \, dt = \int_{I_n} (E\theta_h^n, v_h) \, dt, \quad \forall v_h \in V_h, \; n = 1, \ldots, N_T, \quad (7)$$

$$\int_{I_n} b(u_h^n, q_h) \, dt = 0, \qquad \forall q_h \in Q_h, \; n = 1, \ldots, N_T, \quad (8)$$

$$\int_{I_n} \mathrm{Ra} \; c_1(u_h^{n-1}, \theta_h^n, \psi_h) + c_0(\theta_h^n, \psi_h) \, dt + (\theta_h^n - \theta_h^{n-1}, \psi_h)$$

$$= \int_{I_n} \langle f_n, \psi_h \rangle \, dt + \int_{I_n} (\zeta_h, \psi_h)_{\Gamma_2} \, dt,$$

$$\forall \psi_h \in \Psi_h, \; n = 1, \ldots, N_T. \quad (9)$$

Here a is a bilinear form on $V \times V$ and b is a bilinear form on $V \times Q$ defined by

$$a(v, w) \equiv 2 \sum_{i,j=1}^{d} \int_\Omega D_{ij}(v) D_{ij}(w) \, dx, \qquad b(v, q) \equiv -\sum_{i=1}^{d} \int_\Omega \frac{\partial v_i}{\partial x_i} q \, dx,$$

respectively. Furthermore, c_1 is a trilinear form on $V \times \Psi \times \Psi$ and c_0 is a bilinear form on $\Psi \times \Psi$ defined by

$$c_1(v, \psi, \varphi) \equiv \frac{1}{2} \sum_{i=1}^{d} \int_\Omega v_i \left(\frac{\partial \psi}{\partial x_i} \varphi - \psi \frac{\partial \varphi}{\partial x_i} \right) dx, \qquad c_0(\psi, \varphi) \equiv \sum_{i=1}^{d} \int_\Omega \frac{\partial \psi}{\partial x_i} \frac{\partial \varphi}{\partial x_i} \, dx,$$

respectively. f_h is an approximation to f. L^2-product on the boundary Γ_2 is defined by

$$(r, \psi)_{\Gamma_2} \equiv \int_{\Gamma_2} r\psi \, dx,$$

and ζ_h is considered as an approximation to ζ. The initial condition is given as an approximation to θ^0 in such a way that $\theta_h^0 \in \Psi_h$. According to the equations (1)–(4), initial velocity and initial pressure should be determined from the initial temperature θ_h^0. A set of initial velocity $u_h^0 \in V_h$ and initial pressure $p_h^0 \in Q_h$ are given as a part of solutions to the Stokes equations:

$$a(u_h^0, v_h) + b(v_h, p_h^0) = (E\theta_h^0, v_h), \quad \forall v_h \in V_h,$$

$$b(u_h^0, q_h) = 0, \quad \forall q_h \in Q_h.$$

We use the same notation to represent the inner products in $L^2(\Omega)$ and $(L^2(\Omega))^d$,

$$(\psi, \varphi) \equiv \int_\Omega \psi\varphi\, dx, \quad \psi, \varphi \in L^2(\Omega), \qquad (v, w) \equiv \sum_{i=1}^d \int_\Omega v_i w_i\, dx, \quad v, w \in (L^2(\Omega))^d,$$

which will not cause any confusion.

REMARK 1. If $v \in V$ satisfies $V \cdot v = 0$ in Ω and $v \cdot n = 0$ on Γ, then we have

$$c_1(v, \psi, \varphi) = \int_\Omega (v \cdot \nabla\psi)\varphi\, dx.$$

In order to treat the case where the incompressibility is satisfied only approximately, we employ the trilinear form c_1 defined above to ensure that $c_1(v, \psi, \psi) = 0$ for any functions $v \in V$ and $\psi \in \Psi$.

REMARK 2. The finite element scheme (7)–(9) is essentially the same as the backward Euler method employed for the discretization of time derivative. For the scheme corresponding to the backward Euler method in the case of $\Gamma_2 = \varnothing$, error estimates are performed in [13]. The stability and error analysis in [13] can be extended straightforwardly to the case where $\Gamma_2 \neq \varnothing$.

3.2 A Space-Times Stabilized Finite Element Scheme

The Rayleigh number becomes high if so does the Grashof number. In such case, it is known that some upwind technique is necessary for the stable computation [6], [16], [23]. In this section, we present a stabilized finite element method for the thermal convection with the infinite Prandtl number by applying the method of [10] to the energy equation.

The stabilized finite element scheme for the thermal convection problem with the infinite Prandtl number is formulated as a problem to find $(u_h^n, p_h^n, \theta_h^n; n = 0, \ldots, N_T) \subset V_h \times Q_h \times \Psi_h$ such that

$$\int_{I_n} a(u_h^n, v_h) + b(v_h, p_h^n)\, dt = \int_{I_n} (E\theta_h^n, v_h)\, dt, \quad \forall v_h \in V_h,\ n = 1, \ldots, N_T, \qquad (10)$$

$$\int_{I_n} b(u_h^n, q_h)\, dt = 0, \qquad \forall q_h \in Q_h,\ n = 1, \ldots, N_T, \qquad (11)$$

$$\int_{I_n} \mathrm{Ra}\ c_1(u_h^{n-1}, \theta_h^n, \psi_h) + c_0(\theta_h^n, \psi_h)\, dt$$

$$+ \sum_{K \in \mathfrak{I}_h} \tau_K \int_{I_n} (\mathrm{Ra}\ u_h^{n-1} \nabla \theta_h^n - \Delta \theta_h^n,\ \mathrm{Ra}\ u_h^{n-1} \nabla \psi_h - \Delta \psi_h)_K\, dt$$

$$+ (\theta_h^n - \theta_h^{n-1}, \psi_h) + \sum_{K \in \mathfrak{I}_h} \tau_K (\theta_h^n - \theta_h^{n-1}, \mathrm{Ra}\ u_h^{n-1} \nabla \psi_h - \Delta \psi_h)_K$$

$$= \int_{I_n} \langle f_h, \psi_h \rangle\, dt + \sum_{K \in \mathfrak{I}_h} \tau_K \int_{I_n} \langle f_h, \mathrm{Ra}\ u_h^{n-1} \nabla \psi_h - \Delta \psi_h \rangle_K\, dt + \int_{I_n} (\zeta_h, \psi_h)_{\Gamma_2}\, dt,$$

$$\forall \psi_h \in \Psi_h,\ n = 1, \dots, N_T. \tag{12}$$

The L_2-product in the elements and duality pairing in the elements are denoted by

$$(\psi, \varphi)_K \equiv \int_K \psi \varphi\, dx,$$

$$\langle g, \varphi \rangle_K \equiv \int_K g \varphi\, dx,$$

respectively. The definition of the stability parameter τ_K is formulated as follows [5]:

$$\tau_K \equiv \min \left\{ \frac{h_K}{2\, \mathrm{Ra}|u^{n-1}|_K}, \frac{h_K^2}{12}, \frac{\Delta t}{2} \right\}, \qquad |u^{n-1}|_K \equiv \left(\sum_{i=1}^d |u_{Ki}^{n-1}|^2 \right)^{1/2},$$

$$u_{Ki}^n \equiv \int_K u_{hi}^n\, dx \Big/ \int_K dx,$$

where h_K denotes the diameter of element K. In this paper we do not go into the error estimates of this scheme, which will be discussed in a forthcoming work.

3.3 Sample Simulation

In this section we show numerically that the scheme (10)–(12) works well even for the case of high Rayleigh numbers. A sample problem [13] is defined in the unit square $(-1, 1) \times (-1, 1)$, and in the time interval $(0, 3.2)$. We impose the Diriclet boundary condition on all the boundary, i.e. $\Gamma_2 = \varnothing$. The source term f of the energy equation, initial condition of the temperature, and boundary values of the temperature are given so that the solutions of equations (1)–(4) are as follows:
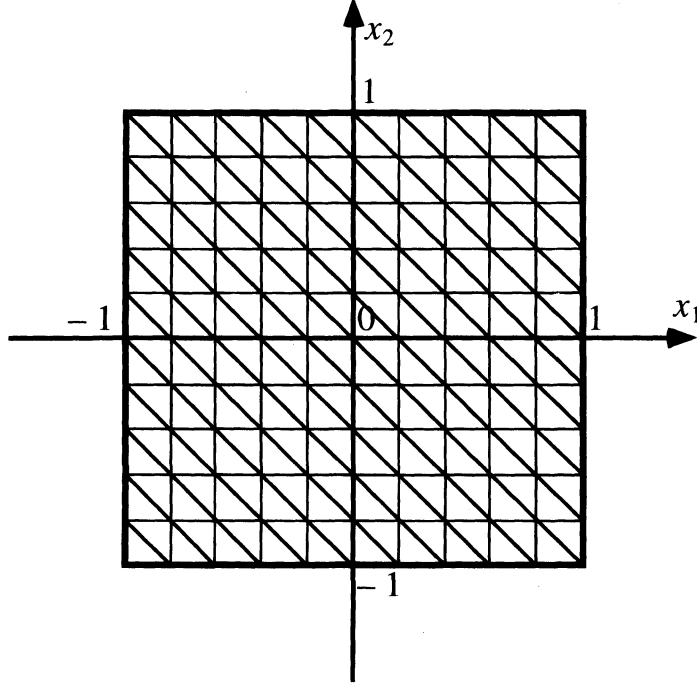
Figure 2: Domain and its subdivision of $N = 10$ in a sample simulation discussed in Section 3.3.

$$u_1 = 0.4t^2(x_1^2 - 1)^2 x_2(x_2^2 - 1), \qquad (13)$$

$$u_2 = -0.4t^2 x_1(x_1^2 - 1)(x_2^2 - 1)^2, \qquad (14)$$

$$p = t^2(0.48x_1^5 x_2 - 3.2x_1^3 x_2 + 4x_1 x_2 + 1.6x_1^3 x_2^3 - 1.6x_1 x_2^3),$$

$$\theta = t^2(0.48x_1^5 - 4.8x_1^3 + 8x_1 + 9.6x_1^3 x_2^2 - 14.4x_1 x_2^2 + 2.4x_1 x_2^4).$$

For the spatial discretization, uniform triangular elements are employed. The domain is divided into a union of $N \times N \times 2$ triangles. With Figure 2, we illustrate a subdivision of the domain in the case of $N = 10$. We use the stabilized finite element scheme (10)–(12) with a P2/P1/P1 finite element approximation to the velocity/pressure/temperature fields.

Computation is performed for different discretization scales $N = 15$ (Case(3.3A)), 20 (Case(3.3B)), 30 (Case(3.3C)) and 40 (Case(3.3D)). The discretization parameters in each case are shown in Table 1. The time increment is set to be $\Delta t = h^2$. Results of the computation are evaluated by means of relative errors,

Table 1.   Computational cases in Section 3.3.

Case		(A)	(B)	(C)	(D)
N		15	20	30	40
h		0.1886	0.1414	0.0943	0.0707
Node Number	u	961	1681	3721	6561
	p, θ	256	441	961	1681

$$\text{Error} - u(H^1) \equiv \frac{\|u - u_h\|_{l^\infty((H^1)^d)}}{\|u\|_{l^\infty((H^1)^d)}},$$

$$\text{Error} - p(L^2) \equiv \frac{\|p - p_h\|_{l^\infty(L^2)}}{\|p\|_{l^\infty(L^2)}},$$

$$\text{Error} - \theta(L^2) \equiv \frac{\|\theta - \theta_h\|_{l^\infty(L^2)}}{\|\theta\|_{l^\infty(L^2)}},$$

where

$$\|v_h\|_{l^\infty(X)} \equiv \max\ \{\|v_h^n\|_X; n = 0, \ldots, N_T\}. \tag{15}$$

We first assume that Ra = 100.   From (13)–(14) we see that the element Peclet number $\text{Pe}_K \equiv \dfrac{\text{Ra}\ |u_K^{n-1}|h_K}{6}$ is about unity.   The relations between the element diameter h and the relative errors are shown in Figure 3.   The slopes obtained from the results in cases (3.3C) and (3.3D) for the velocity, pressure and temperature are 1.957, 2.129 and 1.978, respectively.

We next assume that Ra = 10000.   The element Peclet number Pe_K is about 100.   The relations between the element diameter h and relative errors are shown in Figure 4.   The slopes derived from the results in cases (3.3C) and (3.3D) for the velocity, pressure and temperature are 2.044, 1.756 and 1.335, respectively.   We remark that in every case the computation for Ra = 10000 by means of the non-stabilized scheme (7)–(9) has diverged.

4.   Application to glass manufacturing problems

As an application of the scheme presented in the previous section, we perform numerical simulations in thermal convection problem associated with the infinite Prandtl number.   As stated in the introduction, the aim of this simulation is to make an attempt to clarify the mechanism of thermal convection in the cooling section of glass melting furnaces, and then find a new
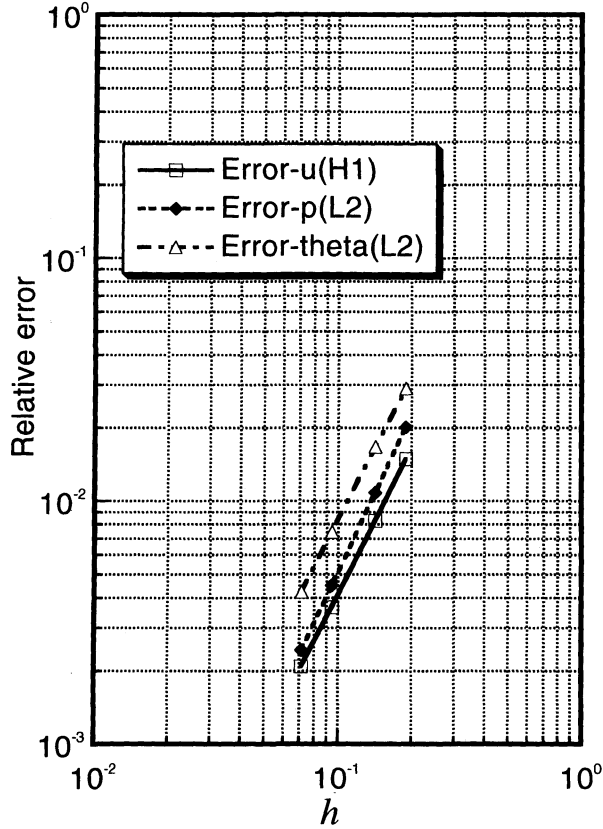
Figure 3: The relative error versus element diameter in a sample simulation in Section 3.3 for Ra = 100.

methods of manufacturing operations in the furnace. In Section 4.2, we investigate the thermal convection phenomena for different kinds of colored glass to clarify the reason for quality debasement in dark colored glass. Next the effect of cooling rates on the convection to avoid the debasement is studied in Section 4.3. Furthermore, in Section 4.4 we present a new cooling method that enables us to shorten a residence time without quality debasement.

4.1 Statement of problem

To investigate the convection phenomena, we discuss a 2-dimensional simplified model of the cooling section. We consider the (dimensional) problem of finding a velocity field $\hat{u}$, a pressure field $\hat{p}$, and a temperature field $\hat{\theta}$ that satisfy, in $\Omega \times (0, \hat{T})$, the equations
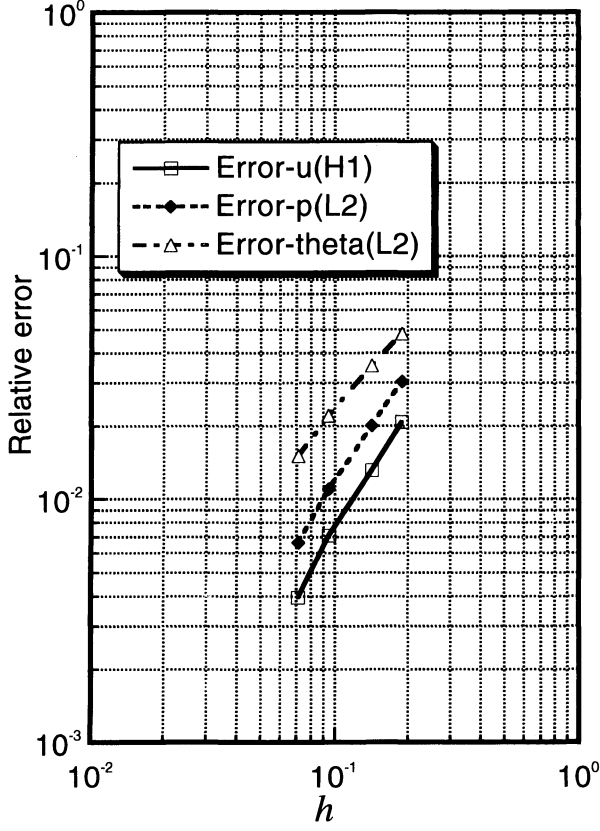
Figure 4:   The relative error versus element diameter in a sample simulation in Section 3.3 for
Ra = 10000.

$$-2\mu\nabla \otimes D(\hat{u}) + \nabla\hat{p} = g\rho\beta E\hat{\theta},$$

$$\nabla \cdot \hat{u} = 0,$$

$$\rho c_p\left(\frac{\partial\hat{\theta}}{\partial\hat{t}} + \hat{u} \cdot \nabla\hat{\theta}\right) = \lambda\Delta\hat{\theta},$$

subject to the initial condition

$$\hat{\theta} = \hat{\theta}^0 \equiv \frac{\hat{\xi}_0}{\lambda}\hat{x}_2 + \hat{\theta}_b, \qquad \text{at } \hat{t} = 0, \tag{16}$$

and boundary conditions

$$\hat{u} = 0, \qquad \hat{\theta} = \hat{\theta}_b, \quad \text{on } \Gamma_b,$$

$$\hat{u}_1 = 0, \quad \frac{\partial \hat{u}_2}{\partial \hat{x}_1} = 0, \quad \frac{\partial \hat{\theta}}{\partial \hat{x}_1} = 0, \qquad \text{on } \Gamma_s,$$

$$\frac{\partial \hat{u}_1}{\partial \hat{x}_2} = 0, \quad \hat{u}_2 = 0, \quad \lambda \frac{\partial \hat{\theta}}{\partial \hat{x}_2} = -\hat{\xi}, \qquad \text{on } \Gamma_t,$$

where ρ, c_p, λ, μ, β are the density, heat capacity, thermal conductivity, viscosity, and the thermal expansion coefficient of the fluid, respectively. The symbol g denotes the gravity acceleration, $\hat{\theta}_b$ is the temperature at the bottom and $\hat{\xi}$ is the cooling rate on the top surface.

The dimensional problem is depicted in Figure 5. At the bottom Γ_b the temperature is fixed to $\hat{\theta}_b$ and the non-slip condition for the velocity is imposed. On both sides Γ_s adiabatic slip condition is imposed to express a periodic boundary condition. On the top Γ_t a free surface condition for the velocity and a heat flux condition for the temperature are imposed. The initial condition (16) is derived from the stationary solution to the problem of top-heated condition with a heat flux $\hat{\xi}_0$:

$$\hat{u} = 0, \quad \hat{p} = g\rho\beta \left\{ \frac{1}{2} \frac{\hat{\xi}_0}{\lambda} \left(\hat{x}_2^2 - \frac{\hat{x}_0^2}{3} \right) + \hat{\theta}_b \left(\hat{x}_2 - \frac{\hat{x}_0}{2} \right) \right\}, \quad \hat{\theta} = \frac{\hat{\xi}_0}{\lambda} \hat{x}_2 + \hat{\theta}_b.$$

This condition is regarded as the temperature distribution formulated in the melting process.

The problem to be discussed is to determine the transient growth of thermal convection in a top-cooled condition, which illustrates a cooling process in a glass melting furnace. The top surface is cooled by heat flux $\hat{\xi}$ in place of the initial heating condition. The interval $[0, \hat{T}]$ is the residence time for glass to pass through the cooling process.

Next we nondimensionalize the problem. We introduce nondimensional variables for the velocity, pressure, temperature, time, cooling rate and length as follows:

$$u = \frac{\hat{u}}{u_0}, \qquad u_0 \equiv \frac{x_0^2 g\rho\beta\theta_0}{\mu} = \text{Ra} \frac{\lambda}{x_0 \rho c_p}, \tag{17}$$

$$p \equiv \frac{\hat{p}}{p_0} - \frac{\hat{\theta}_b}{\theta_0} (x_2 - 0.5), \qquad p_0 = x_0 g\rho\beta\theta_0 = \text{Ra} \frac{\mu\lambda}{x_0^2 \rho c_p}, \tag{18}$$

$$\theta \equiv \frac{\hat{\theta} - \hat{\theta}_b}{\theta_0}, \quad \theta_0 = \frac{x_0 \xi_0}{\lambda}, \tag{19}$$

$$t \equiv \frac{\hat{t}}{t_0}, \quad t_0 = \frac{x_0^2 \rho c_p}{\lambda}, \tag{20}$$

$$\Gamma_b : \hat{u}_1 = 0, \hat{u}_2 = 0, \hat{\theta} = \hat{\theta}_b$$

$$\Gamma_s : \hat{u}_1 = 0, \frac{\partial \hat{u}_2}{\partial \hat{x}_1} = 0, \frac{\partial \hat{\theta}}{\partial \hat{x}_1} = 0$$

$$\Gamma_t : \hat{u}_2 = 0, \frac{\partial \hat{u}_1}{\partial \hat{x}_2} = 0, \lambda \frac{\partial \hat{\theta}}{\partial \hat{x}_2} = -\hat{\xi}$$
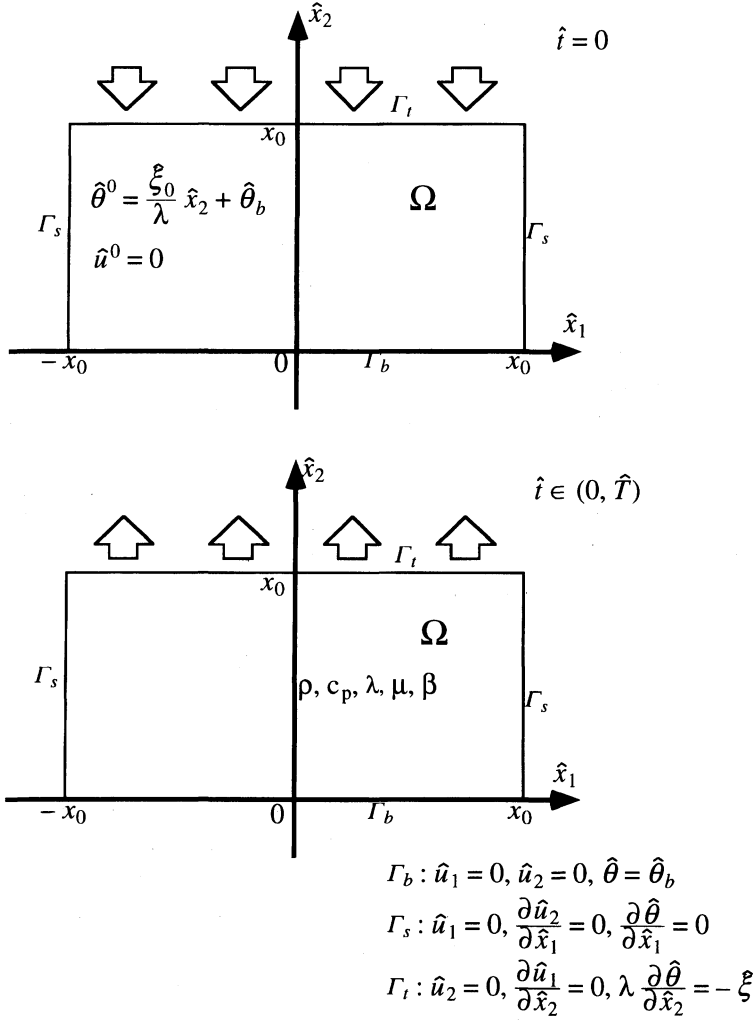
Figure 5: The depiction of the dimensional problem in Section 4.1.

$$\xi \equiv \frac{\hat{\xi}}{\xi_0}, \qquad \xi_0 = \hat{\xi}_0, \tag{21}$$

$$x \equiv \frac{\hat{x}}{x_0}, \tag{22}$$

where x_0 is the depth of the cooling section.   Rayleigh number is defined to be

$$\text{Ra} \equiv \frac{x_0^3 g \rho^2 \beta c_p \theta_0}{\mu \lambda} = \frac{x_0^4 g \rho^2 \beta c_p \xi_0}{\mu \lambda^2}. \tag{23}$$

Thus we are lead to the (nondimensional) problem of finding a velocity field u, pressure field p, and temperature field θ that satisfy, in $\Omega \times (0, T)$, the equations

$$-2\nabla \otimes D(u) + \nabla p = E\theta,$$

$$\nabla \cdot u = 0,$$

$$\frac{\partial \theta}{\partial t} + \text{Ra } u \cdot \nabla \theta = \Delta\theta,$$

with the initial condition

$$\theta = \theta^0 = x_2, \qquad \text{at } t = 0,$$

and the boundary conditions

$$u = 0, \qquad \theta = 0, \qquad\qquad\qquad \text{on } \Gamma_b$$

$$u_1 = 0, \qquad \frac{\partial u_2}{\partial x_1} = 0, \qquad \frac{\partial \theta}{\partial x_1} = 0, \quad \text{on } \Gamma_s$$

$$\frac{\partial u_1}{\partial x_2} = 0, \quad u_2 = 0, \qquad \frac{\partial \theta}{\partial x_2} = -\xi, \quad \text{on } \Gamma_t.$$

Setting $\Gamma_1 = \Gamma_b$, $\Gamma_2 = \Gamma_s \cup \Gamma_t$ and

$$f = 0, \quad \zeta = \begin{cases} 0 & \text{on } \Gamma_s, \\ -\xi & \text{on } \Gamma_t, \end{cases}$$

the problem is reduced to (1)–(6).

The nondimensional problem is depicted in Figure 6. From (17)–(23) the dependence of the Rayleigh number and scaling values on the thermal conductivity λ is expressed as

$$\text{Ra } \propto \lambda^{-2}, \qquad \theta_0 \propto \lambda^{-1},$$

$$\mu_0 \propto \lambda^{-1}, \qquad p_0 \propto \lambda^{-1},$$

$$t_0 \propto \lambda^{-1}.$$

The conditions for the numerical simulation is as follows. As for the spatial discretization, uniform triangular elements are adopted. The domain is divided into $N \times 2N \times 2$ triangles, where $N = 40$. We employ the stabilized finite elements scheme (10)–(12) with P2/P1/P1 finite element approximation to the velocity/pressure/temperature fields. A slight perturbation is added to the cooling rate ξ to induce thermal convection:

$$\xi' = \xi + 0.01 \times \cos\left(2\pi\frac{x_1}{20}\right).$$
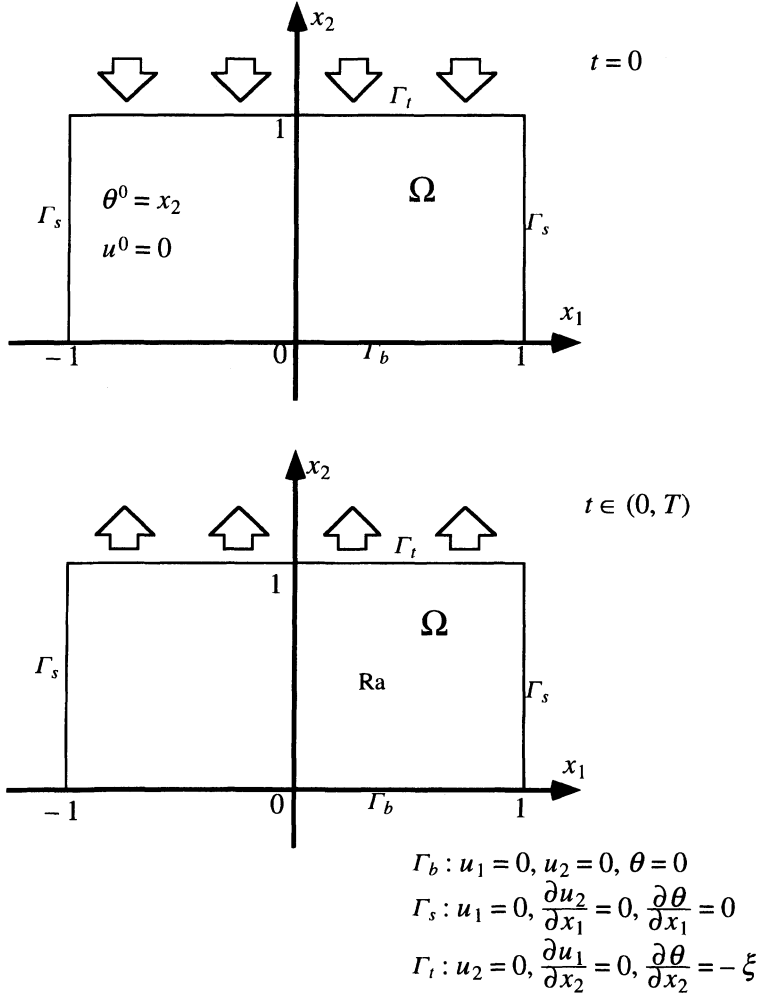
Figure 6:   The depiction of the nondimensional problem in Section 4.1.

Under the conditions mentioned above, we perform numerical simulations for different thermal conductivities λ and cooling rates ξ.

4.2   Numerical Simulation (1) – The Effect of Thermal Conductivity

First we investigate the thermal convection of top-cooled problems for different kinds of colored molten glass.   Computation is performed to simulate typical cooling processes in glass melting furnaces for 4 different glass colors whose thermal conductivities are:

Case (4.2A) $\lambda = \lambda_0 \ (= 60[\mathrm{W/mK}])$ clear glass,

Case (4.2B) $\lambda = \frac{1}{2}\lambda_0,$

Case (4.2C) $\lambda = \frac{1}{4}\lambda_0,$

Case (4.2D) $\lambda = \frac{1}{8}\lambda_0,$ dark gray glass.

The dimensional depth of furnace x_0 is 1[m]. The dimensional residence time in the cooling process is 3912[s] in each case. The corresponding Rayleigh number and time interval of the nondimensional problem are:

Case (4.2A) $\mathrm{Ra} = 1 \times 10^5,$ $T = 8 \times 10^{-2},$ $\Delta t = 1 \times 10^{-4},$

Case (4.2B) $\mathrm{Ra} = 4 \times 10^5,$ $T = 4 \times 10^{-2},$ $\Delta t = 5 \times 10^{-5},$

Case (4.2C) $\mathrm{Ra} = 1.6 \times 10^6,$ $T = 2 \times 10^{-2},$ $\Delta t = 2.5 \times 10^{-5},$

Case (4.2D) $\mathrm{Ra} = 6.4 \times 10^6,$ $T = 1 \times 10^{-2},$ $\Delta t = 1.25 \times 10^{-5}.$

The cooling rate on the top surface is $\xi = 2$ in each case, which is a normal cooling rate in the cooling section of the standard glass melting furnace.

In Figures 7 to 10, the temperature field, velocity field and streamlines at $t = T$ in the cases of (4.2A) to (4.2D) are shown, respectively. The streamlines in each case are loci of particles in $(0, \ T)$ initially placed on the line of $x_2 = 0.95$. From Figures 7 to 10, the growth of the convection cells is observed at $t = T$ in each case. In Figure 11 the relation between time t and the maximum velocity $\|u_h^n\|_\infty$ in case(4.2D) is shown, where $\|u_h^n\|_\infty$ is defined by

$$\|u_h^n\|_\infty \equiv \max_{x \in \Omega} |u_h^n|, \qquad |u_h^n| \equiv \left(\sum_{i=1}^d u_{h_i}^{n2} \right)^{1/2}. \qquad (24)$$

Figure 12 shows the relation between time t and the difference of the maximum velocity $\|u_h^n\|_\infty - \|u_h^{n-1}\|_\infty$. In early stage, there exist no visible convections in each case. At $t = 0.475T$ in case(4.2D), the onset of thermal convection is seen as a sudden increase of the maximum velocity $\|u_h^n\|_\infty$ as is shown in Figure 12. After that the maximum velocity $\|u_h^n\|_\infty$ continues increasing, which indicates the growth of thermal convection. Figure 13 shows the relation between thermal conductivity λ and the onset time t_c. The onset time t_c is determined as a time when sudden increase of $\|u_h^n\|_\infty$ occurs. From Figure 13, we see that there exists a relation of $t_c \propto \lambda$, which means that the dimensional time of onset is almost identical for every case. This relation can be explained from the growth of thermal boundary layer on the top surface by cooling. In the thermal conduction problem of semi-infinite solid, the

Hajime Iтон

A	0.000
B	0.050
C	0.100
D	0.150
E	0.200
F	0.250
G	0.300
H	0.350
I	0.400
J	0.450
K	0.500
L	0.550
M	0.600
N	0.650
O	0.700
P	0.750
Q	0.800
R	0.850
S	0.900
T	0.950
U	1.000
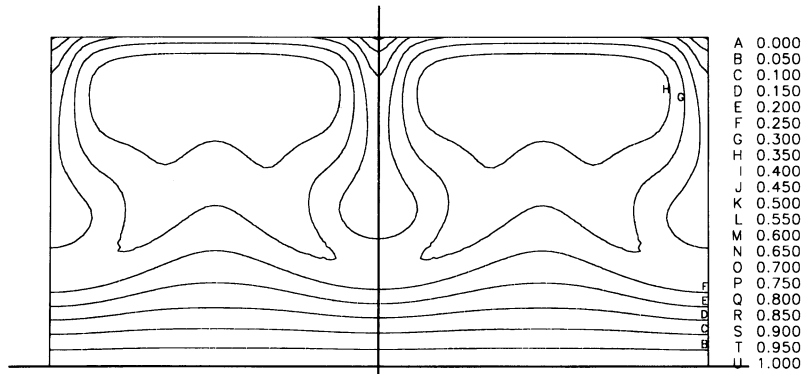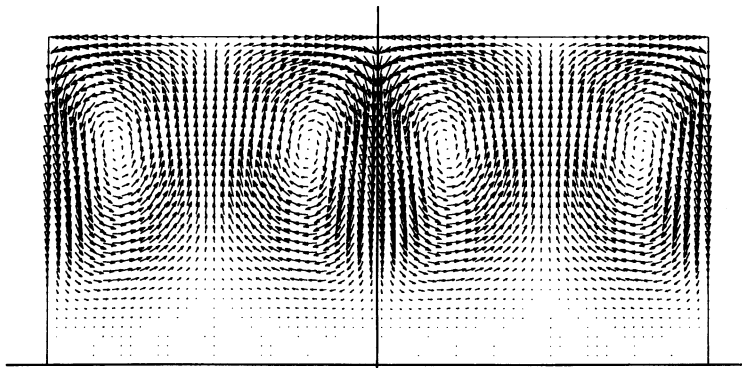
Temperature
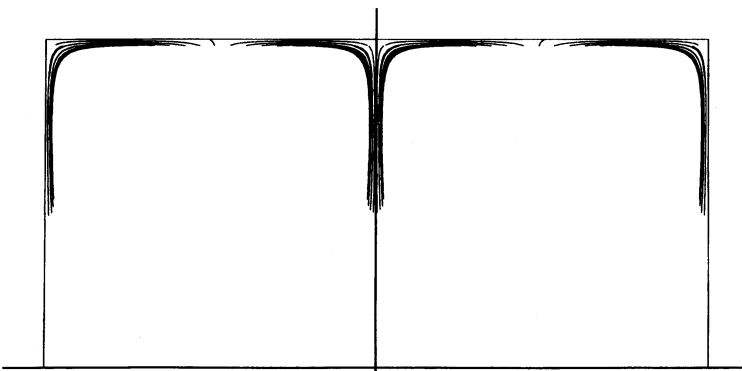
Velocity

Streamlines

Figure 7: Computational results at $t = T$ in case of (4.2A).

Temperature

A	0.000
B	0.050
C	0.100
D	0.150
E	0.200
F	0.250
G	0.300
H	0.350
I	0.400
J	0.450
K	0.500
L	0.550
M	0.600
N	0.650
O	0.700
P	0.750
Q	0.800
R	0.850
S	0.900
T	0.950
U	1.000
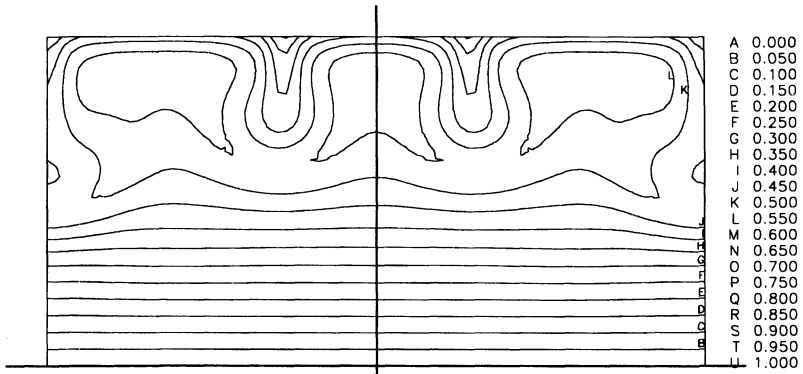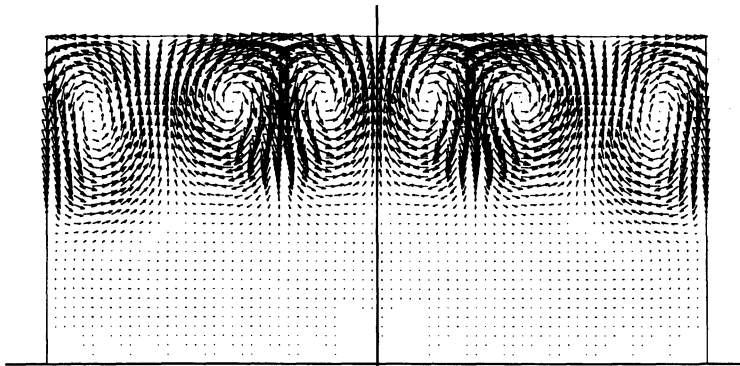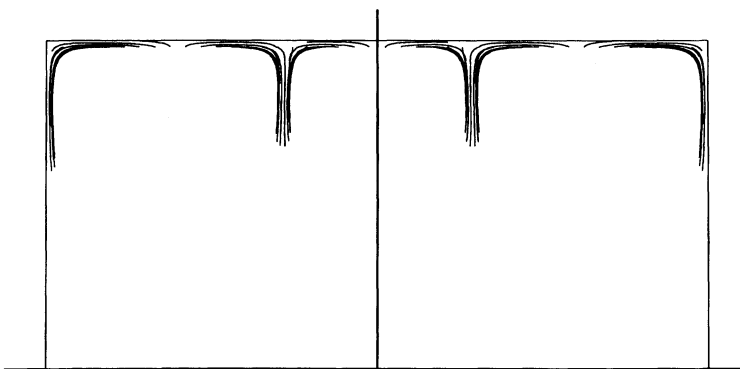
Velocity

Streamlines

Figure 8: Computational results at $t = T$ in case of (4.2B).

Temperature

A	0.000
B	0.050
C	0.100
D	0.150
E	0.200
F	0.250
G	0.300
H	0.350
I	0.400
J	0.450
K	0.500
L	0.550
M	0.600
N	0.650
O	0.700
P	0.750
Q	0.800
R	0.850
S	0.900
T	0.950
U	1.000
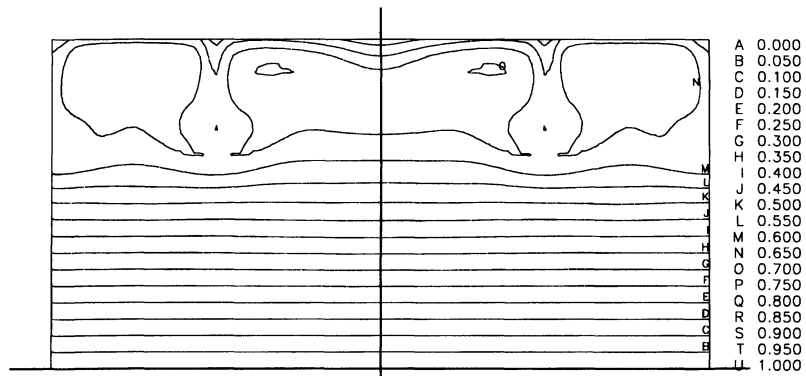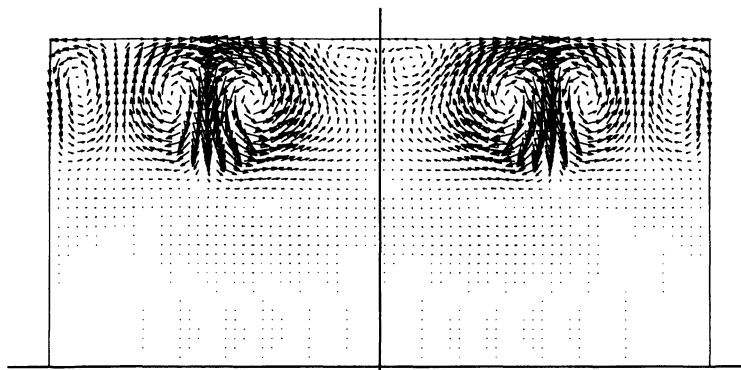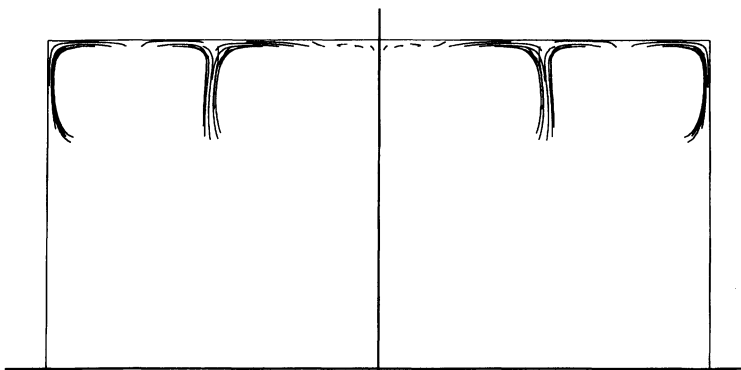
Velocity

Streamlines

Figure 9:   Computational results at $t = T$ in case of (4.2C).
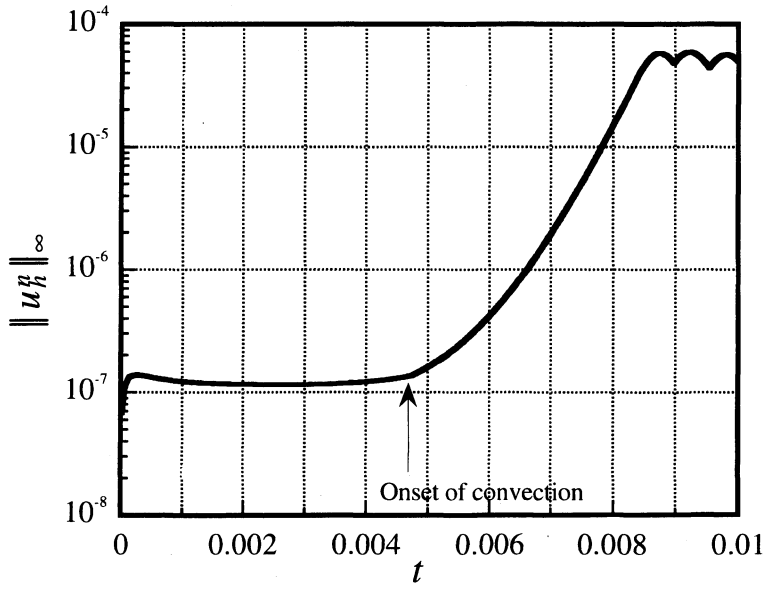
Figure 11: The relation between time t and the maximum velocity $\|u_h^n\|_\infty$ in case of (4.2D).
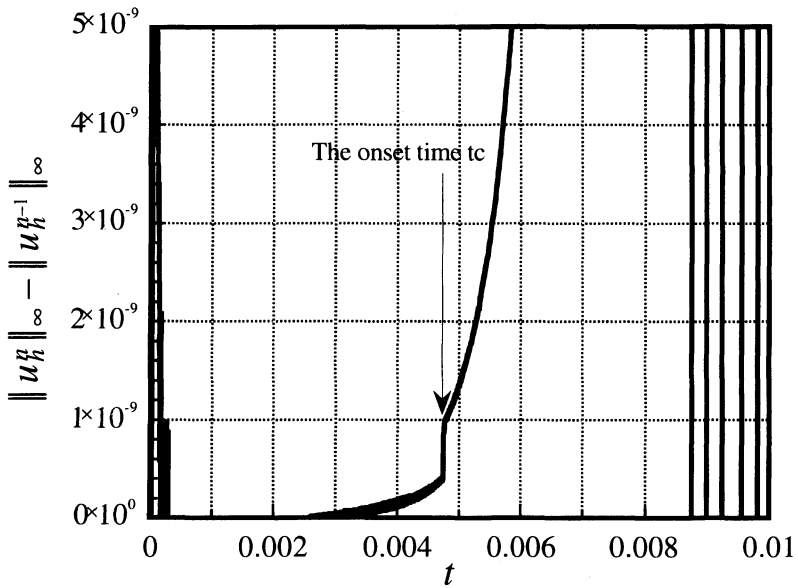
Figure 12: The dependence of the difference of the maximum velocity $\|u_h^n\|_\infty - \|u_h^{n-1}\|_\infty$ on time t in case of (4.2D).

A	0.000
B	0.050
C	0.100
D	0.150
E	0.200
F	0.250
G	0.300
H	0.350
I	0.400
J	0.450
K	0.500
L	0.550
M	0.600
N	0.650
O	0.700
P	0.750
Q	0.800
R	0.850
S	0.900
T	0.950
U	1.000

Temperature

Velocity

Streamlines
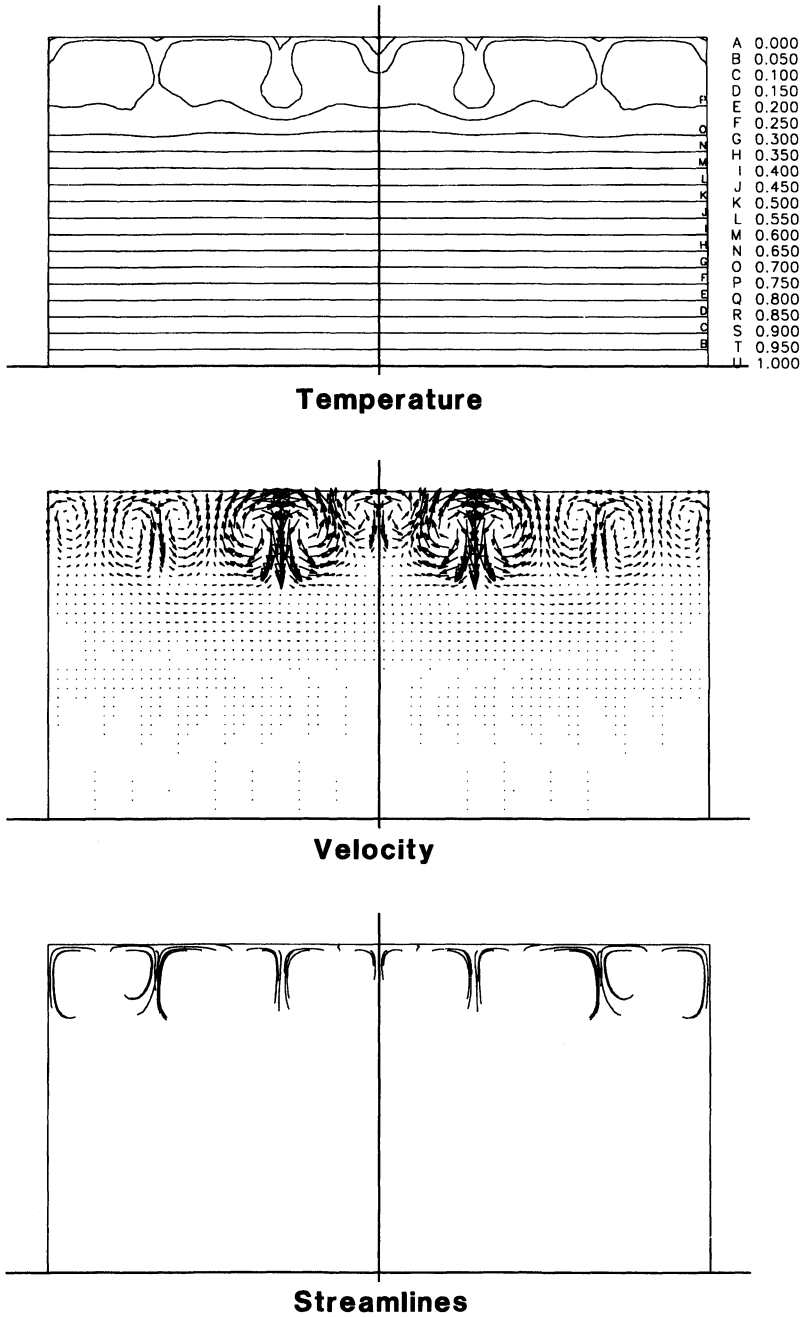
Figure 10: Computational results at $t = T$ in case of (4.2D).
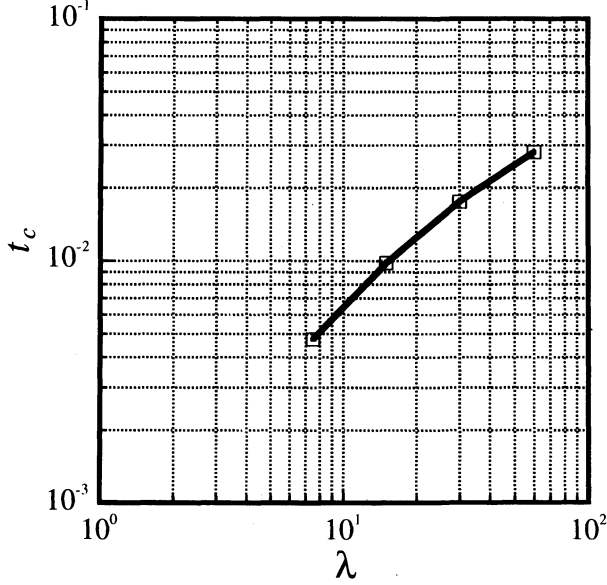
Figure 13: The relation between thermal conductivity λ and onset time t_c in Section 4.2.

boundary thickness δx and the temperature difference $\delta\theta$ of the boundary layer are known to be proportional to the square-root of the time [3]. When we take the local Rayleigh number $\text{Ra}l$ to be $\text{Ra}l \equiv \text{Ra}\,\delta x^3 \delta\theta$, the local Rayleigh number enjoys the relation $\text{Ra}l \propto \text{Ra}\,t^2$. The onset time is thought to be the time when the local Rayleigh number attains the critical Rayleigh number Rac. Hence $t_c \propto \left(\dfrac{\text{Rac}}{\text{Ra}}\right)^{1/2} \propto \lambda$ is obtained in the semi-infinite problem. In case of high Rayleigh numbers, the boundary layer thickness is $\delta x \ll 1$ at the onset time, and it is considered that the same relation as in the semi-infinite problem holds.

In Figure 14, the relation between the thermal conductivity λ and the number N_c of roll cells is shown. The number N_c, which is inversely proportional to the size of roll cells, is almost proportional to $\lambda^{-1/2}$. This is explained from the fact that the boundary layer thickness at the onset time follows the relation of $\delta x \propto t_c^{1/2} \propto \lambda^{1/2}$, and the size of roll cells is thought to be proportional to the boundary layer thickness at the onset time of the thermal convection.

From these results we see that in case of low Rayleigh numbers (clear glass) there exist large Rayleigh-Benard cells whose number is small, while in case of high Rayleigh numbers (dark glass) a large number of small roll cells develop under the surface, which would debase the glass quality.
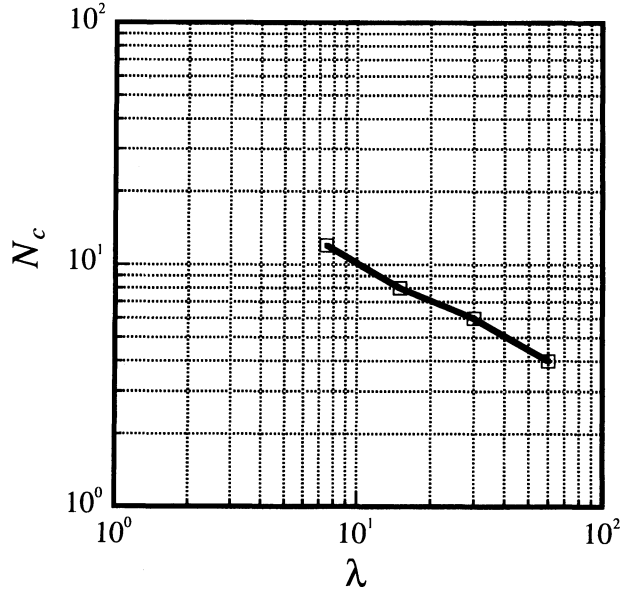
Figure 14: The relation between thermal conductivity λ and number of roll cells N_c in Section 4.2.

Table 2.   Computational cases in Section 4.3.

Case	(A)	(B)	(C)	(D)	(E)	(F)
ξ_1	0.00	0.50	0.75	1.00	1.25	1.50
$T(\xi_1)_{(\times 10^{-2})}$	3.0000	2.0000	1.7250	1.5000	1.3375	1.2000
Case	(G)*	(H)	(I)	(J)	(K)	(L)
ξ_1	2.00	2.50	3.00	4.00	6.50	11.00
$T(\xi_1)_{(\times 10^{-2})}$	1.0000	0.8625	0.7500	0.6000	0.4000	0.2500

*: same as (4.2D)

4.3   Numerical Simulation (2)—The Effect of Cooling Rate

    Next, we investigate the relation between the growth of thermal convection
and cooling rate ξ in the case of dark gray glass (case (4.2D)).   The purpose of
this simulation is to find an optimal cooling rate for which the appearance of
Rayleigh-Benard cells is avoided.   With the same Rayleigh number Ra and the
same time increment Δt as those of case (4.2D), we perform computations of
12 cases for different cooling rates $\xi = \xi_1$, as shown in Table 2.   The case of
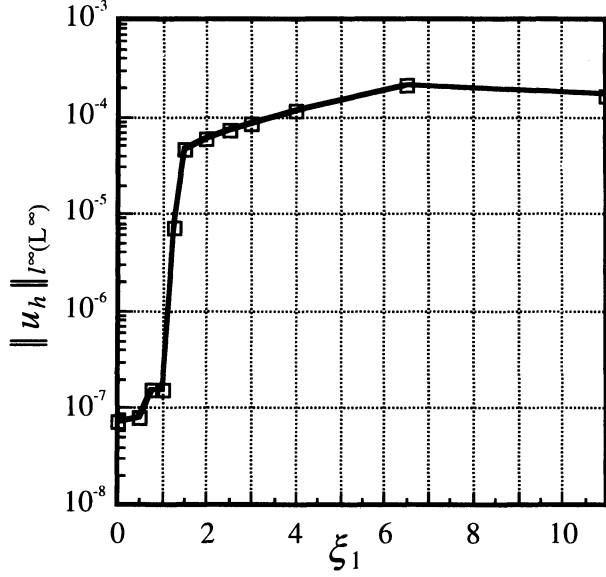
Figure 15: The relation between cooling rate ξ_1 and maximum velocity $\|u_h\|_{l^\infty(L^\infty)}$ in the time interval in Section 4.3.

$\xi_1 = 2$ corresponds to the case (4.2D). The ending time $T(\xi_1)$ is determined to be

$$T(\xi_1) = \frac{2+1}{\xi_1 + 1} T_0,$$

where $T_0 = 0.01$ is the time interval for case (4.2D), so that the total amount of energy consumption in the interval $[0, T(\xi_1)]$ is almost equal in all cases. This equation is derived in the following way. The heat flux $\dfrac{\partial \theta}{\partial x_2}$ on Γ_b is considered to be approximately 1 because the temperature gradient at the bottom remains unchanged, keeping the initial temperature gradient 1 in the whole time interval $[0, T(\xi_1)]$. Hence the total flux that goes out of the domain is nearly equal to $\xi_1 + 1$. Since the total energy consumption in case (4.2D) is $(2 + 1)T_0$, we obtain the equation shown above.

Figure 15 shows the relation between the cooling rate ξ_1 and the maximum velocity $\|u_h\|_{l^\infty(L^\infty)}$ in $[0, T(\xi_1)]$ defined in (15) and (24). The maximum velocity $\|u_h\|_{l^\infty(L^\infty)}$ increases suddenly at $\xi_1 = 1.25$. We now look at the states of thermal convection in detail. In Figures 16 to 18, the computational results of the temperature field, velocity field and streamlines at $t = T$ in cases of $\xi_1 = 1$, 1.25 and 1.5 are shown, respectively. We also refer to Figure 10 for the result of $\xi_1 = 2$. In case $\xi_1 \le 1$, thermal convection is not seen and

particles hardly move (Figure 16). When $\xi_1 = 1.25$ particles show a slight movement (Figure 17). In case $\xi_1 \geq 1.5$, the growth of convection cells is observed and the movement of particles indicates the formation of roll cells (Figures 10 and 18). Formation of roll cells like this is a cause of optical distortion on the surface of glass. Therefore the choice $\xi_1 \leq 1.25$ is one of the ways to avoid the debasement of glass quality.

We now introduce the relative onset time $\chi_0 \equiv t_c/T$. Figure 19 shows the relation between the cooling rate ξ_1 and relative onset time χ_0, and that χ_0 takes its minimum value 0.45 at $\xi_1 = 2.5$. That is, for any cooling rate ξ_1, the onset of thermal convection never occurs before the time $0.45 \times T(\xi_1)$. This is an idea of obtaining a new cooling method which can produce glass without quality debasement in a short residence time. This method is presented in the next subsection.

4.4 Numerical Simulation (3)—The Time-Dependent Cooling Rate

From the results in Section 4.3, the debasement of glass quality caused by top-cooling can be avoided if the cooling rate is taken to be $\xi_1 \leq 1.25$. However, from the viewpoint of the process design and manufacturing operations, the decrease of cooling rate brings about the need of the increase in residence time, for which the magnification of the cooling section is necessary. Our plan is to perform further simulations to find new cooling methods which may be applied to the glass production without quality debasement in a short residence time.

Let v^* be the maximum velocity $\|u_h\|_{l^\infty(L^\infty)}$ and T^* be the ending time in the case (4.3E). We consider a problem of finding a cooling rate $\xi = \xi(t)$ such that the ending time T is less than T^* and the maximum velocity $\|u_h\|_{l^\infty(L^\infty)}$ is less than v^*. As a choice of $\xi(t)$, we present a 2-step time-dependent cooling method involving 3 parameters ξ_1, ξ_2 and χ:

$$\xi(t) = \begin{cases} \xi_1 \ (0 \leq t \leq T_1(\xi,\chi)), \\ \xi_2 \ (T_1 < t \leq T(\xi_1,\xi_2,\chi)), \end{cases}$$

$$T_1(\xi_1,\chi) \equiv \chi \frac{2+1}{\xi_1+1} T_0, \quad T(\xi_1,\xi_2,\chi) \equiv T_1(\xi_1,\chi) + (1-\chi)\frac{2+1}{\xi_2+1} T_0,$$

where $\xi_2 < 1.25 < \xi_1$ and $0 < \chi < 0.45$. The reason for the choice of this cooling method is based on the results of Section 4.3. The thermal convection does not occur in the first step $0 \leq t \leq T_1(\xi_1,\chi)$ with any ξ_1 for $\chi < 0.45$. If larger cooling rates ξ_1 are taken, it may be possible to shorten the interval of the first step. On the other hand, the second cooling rate ξ_2 is less than 1.25, and so the thermal convection may not occur in the whole time interval if we

|	
A	0.000
B	0.050
C	0.100
D	0.150
E	0.200
F	0.250
G	0.300
H	0.350
I	0.400
J	0.450
K	0.500
L	0.550
M	0.600
N	0.650
O	0.700
P	0.750
Q	0.800
R	0.850
S	0.900
T	0.950
U	1.000

Temperature

Velocity

Streamlines
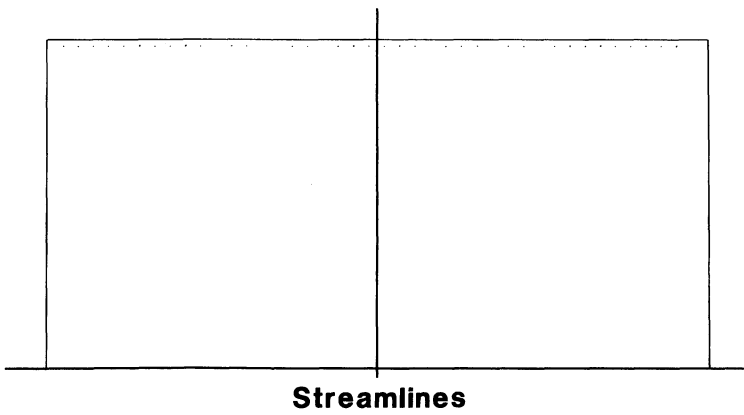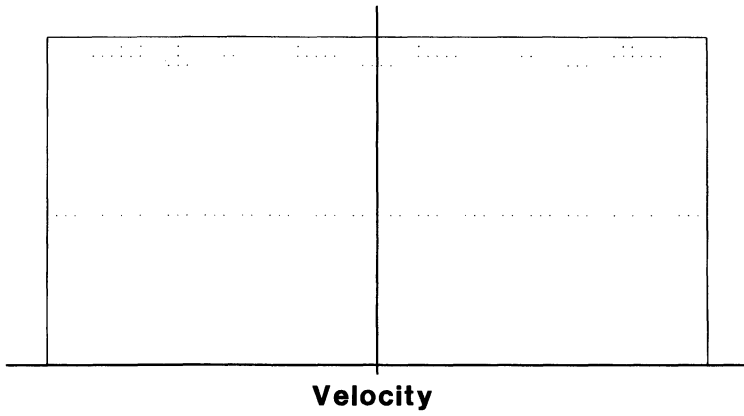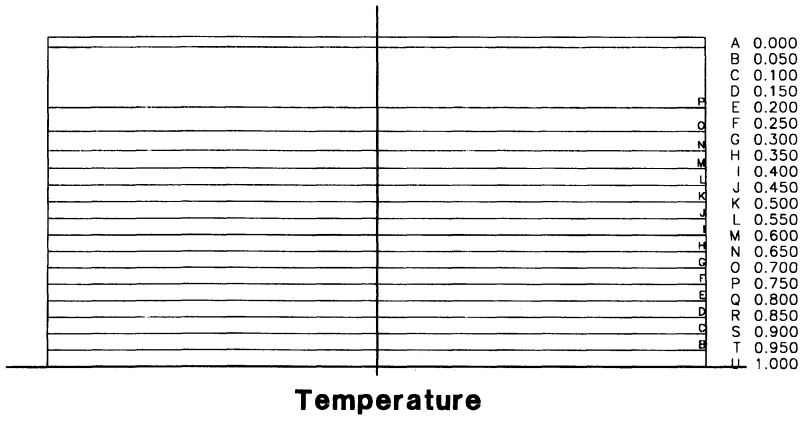
Figure 16: Computational result at $t = T$ in case of $\xi_1 = 1$ (case (4.3D)) in Section 4.3.

Temperature

A	0.000
B	0.050
C	0.100
D	0.150
E	0.200
F	0.250
G	0.300
H	0.350
I	0.400
J	0.450
K	0.500
L	0.550
M	0.600
N	0.650
O	0.700
P	0.750
Q	0.800
R	0.850
S	0.900
T	0.950
U	1.000
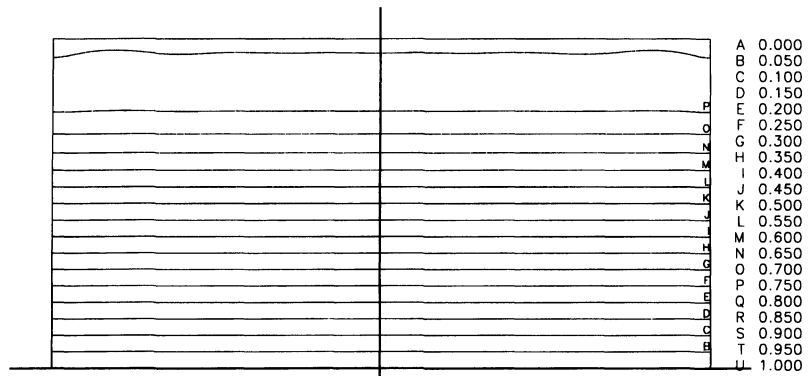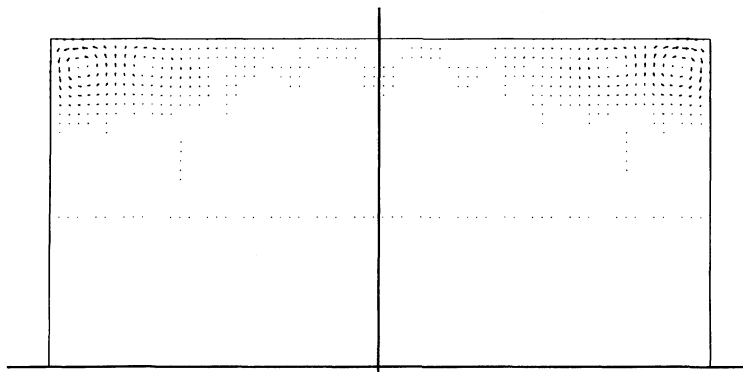
Velocity
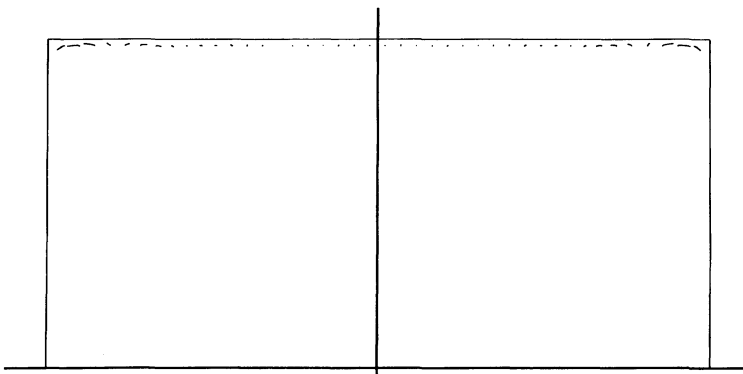
Figure 17: Computational result at $t = T$ in case of $\xi_1 = 1.25$ (case (4.3E)) in Section 4.3.

A	0.000
B	0.050
C	0.100
D	0.150
E	0.200
F	0.250
G	0.300
H	0.350
I	0.400
J	0.450
K	0.500
L	0.550
M	0.600
N	0.650
O	0.700
P	0.750
Q	0.800
R	0.850
S	0.900
T	0.950
U	1.000

Temperature

Velocity

Streamlines
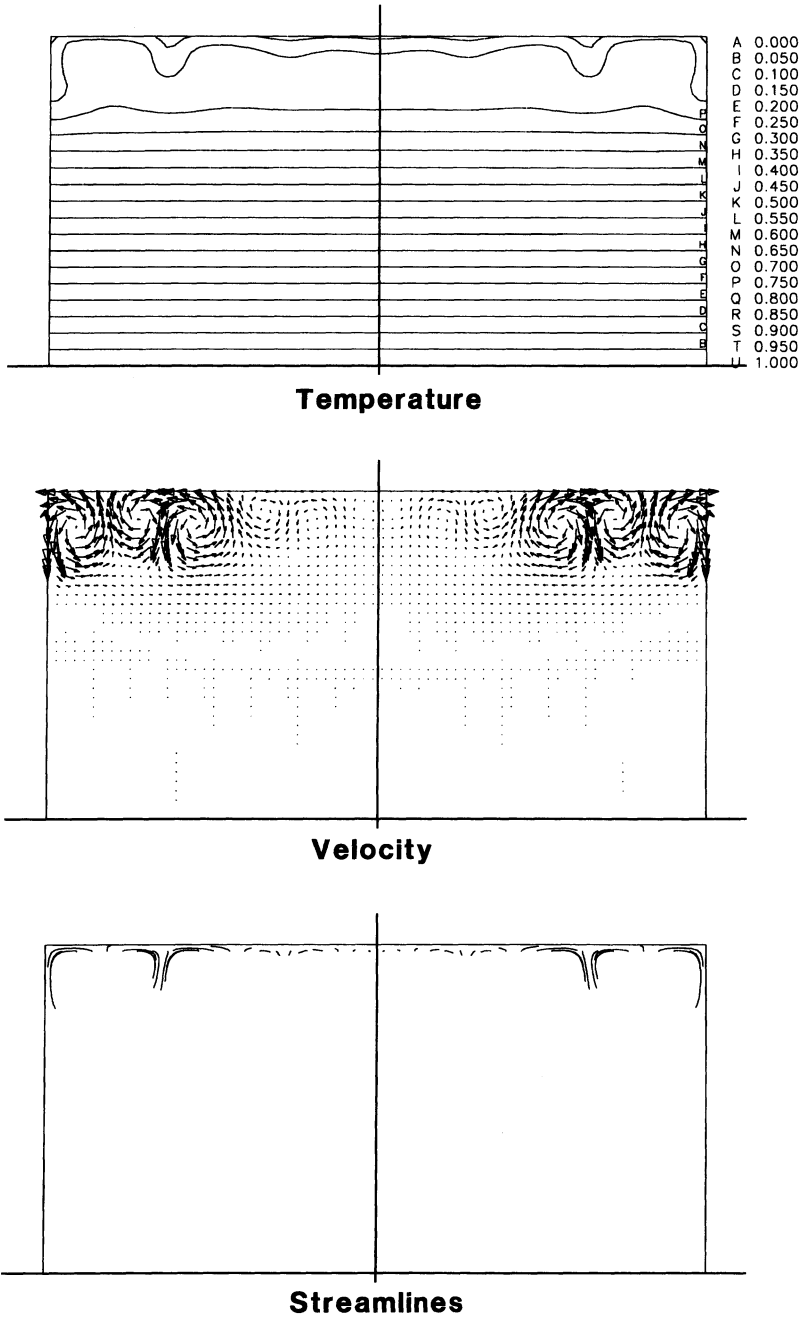
Figure 18: Computational result at $t = T$ in case of $\xi_1 = 1.5$ (case (4.3F)) in Section 4.3.
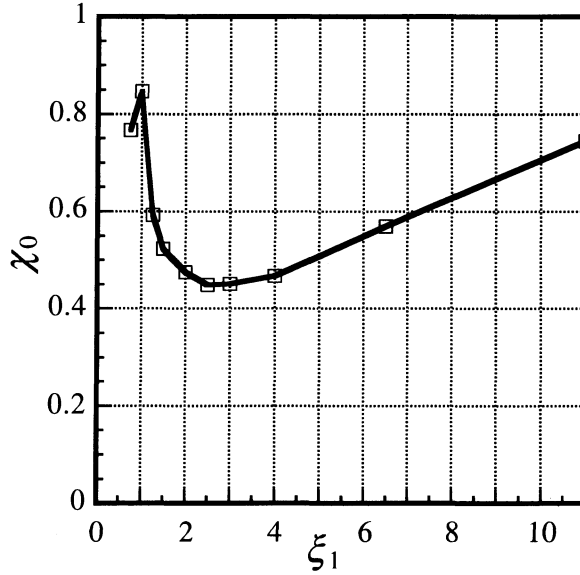
Figure 19:   The relation between cooling rate ξ_1 and relative onset time χ_0 in thermal convection in Section 4.3.

Table 3.   Computational cases in Section 4.4.

Case	(A)	(B)	(C)	(D)	(E)	(F)
ξ_1	4.00	6.50	11.00	4.00	6.50	11.00
χ	0.2	0.2	0.2	0.3	0.3	0.3
$T_{1(\times 10^{-2})}$	0.120	0.080	0.050	0.180	0.120	0.075
$T_{(\times 10^{-2})}$	1.3250	1.2875	1.2500	1.2375	1.1750	1.1250

$T^* : 1.3750 \times 10^{-2}$

take an appropriate ξ_2.   Thus the cooling method presented above has the possibility of shortening the residence time $[0, T]$ without causing thermal convection.   The cooling rate in the second step ξ_2 is chosen to be 1 in our computation.

With the Rayleigh number Ra and the time increment Δt of case (4.3E), we perform computation of 6 cases for the different values of ξ_1 and χ as shown in Table 3.   Results are evaluated by the maximum velocity $\|u_h\|_{l^\infty(L^\infty)}$ in comparison with v^*.   The relation between time and cooling rate in cases (4.3E) and (4.4C) is shown in Figure 20.   We remark that T of all the cases is less than T^*.
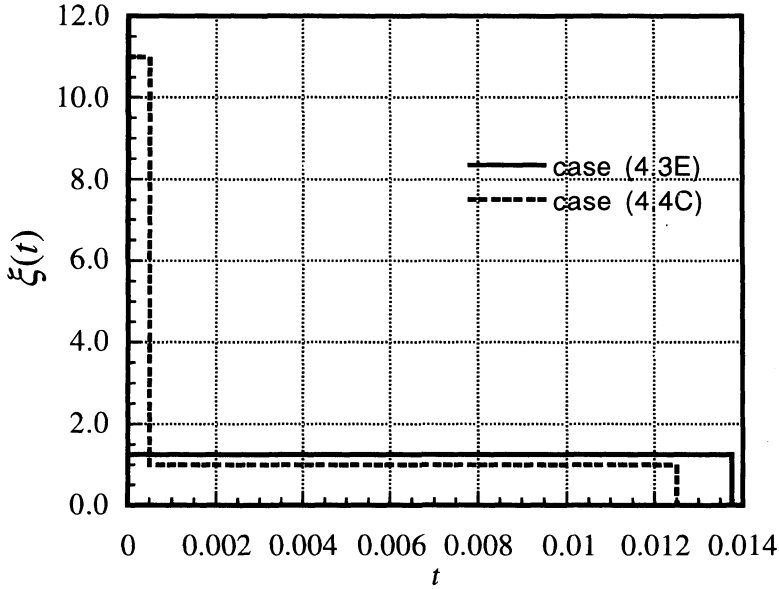
Figure 20: The relation between time t and cooling rate $\xi(t)$ in cases (4.3E) and (4.4C).

In Table 4, the maximum velocity $\|u_h\|_{l^\infty(L^\infty)}$ in different values ξ_1 and χ are presented. When $\chi = 0.2$, the maximum velocity $\|u_h\|_{l^\infty(L^\infty)}$ is less than v^* in each cooling rate. When $\chi = 0.3$, the maximum velocity $\|u_h\|_{l^\infty(L^\infty)}$ is greater than v^* in each cooling rate. Therefore we could propose that our cooling method presented here makes it possible to shorten the time interval without quality debasement in comparison with constant cooling $\xi_1 = 1.25$ in Section 4.3, if we take χ to be appropriate, e.g., $\chi = 0.2$ in our computations.

5. Conclusions

Thermal convection phenomena in fluids with the infinite Prandtl number, which gives a model of the cooling sections in glass melting furnaces, have been discussed via numerical simulations. The stabilized finite element scheme for the thermal convection problem with the infinite Prandtl number was presented to treat problems with high Rayleigh numbers. By means of this scheme, transient growth of thermal convection in a cooling process in a glass melting furnace has been studied. The computational results revealed the mechanism of the generation of thermal convection on cooling process as shown in the following:

  − A lot of roll cells develop just under the surface in case of dark colored glass.

Table 4. Computational results
$\|u_h\|_{l^\infty(L^\infty)}$ in Section 4.4.

ξ_1	χ	
	0.2	0.3
4.00	6.309×10^{-7}	8.713×10^{-6}
6.50	1.084×10^{-6}	2.068×10^{-5}
11.00	1.091×10^{-6}	1.959×10^{-5}

V^*: 6.959×10^{-6}

– The onset time of thermal convection is almost identical in real time for any λ. The size of rolls is proportional to $\lambda^{1/2}$.
– There exists a value of cooling rate $\xi_1 = 1.25$ under which thermal convection does not occur in the cooling interval. To set $\xi_1 \leq 1.25$ is a way to avoid the debasement of glass quality.
– For any cooling rate ξ_1, the onset of thermal convection never occurs before the time $0.45 \times T(\xi_1)$, where $T(\xi_1)$ is the ending time defined in Section 4.3. This can be an idea of presenting a new cooling method which can produce glass without debasement of quality in a shorter residence time.

Based on the computational results shown above, a new time-dependent cooling method which has 2 steps of different cooling rates, the strong cooling in the first step and the mild cooling in the second, was presented. the computational results made it clear that we can shorten a residence time necessary for cooling without the debasement of glass quality by using this method.

Acknowledgments

References

[1] J. Boland and W. Layton, An analysis of the finite element method for natural convection problems, Numerical Methods for Partial Differential Equations **2** (1990), 115–126.

[2]   J. Boland and W. Layton,   Error analysis for finite element methods for steady natural convection problems,   Numerical Functional Analysis and Optimization 11 (1990), 449–483.

[3]   H. Carslow and J. Jaeger,   Conduction of Heat in Solids, 2nd edition,   Oxford University Press, Oxford, 1959.

[4]   A. Chorin,   A numerical method for solving incompressible viscous flow problems,   Journal of Computational Physics 2 (1967) 12–26.

[5]   L. P. Franca, S. L. Frey and T. J. R. Hughes,   Stabilized finite element methods: I. Application to the advective-diffusive model,   Computer Methods in Applied Mechanics and Engineering 95 (1992) 253–276.

[6]   S. Fujima, M. Tabata and Y. Fukasawa,   Extension to three-dimensional problems of the upwind finite element scheme based on the choice of up- and downwind points,   Computer Methods in Applied Mechanics and Engineering 112 (1994), 109–131.

[7]   V. Girault and P. A. Raviart,   Finite Element Methods for Navier-Stokes Equations, Theory and Algorithms, Springer, Berlin, 1986.

[8]   U. Hansen and A. Ebel,   Time-dependent thermal convection: a possible explanation for a multiscale flow in the earth's mantle,   Geophysical Journal 94 (1988), 181–191.

[9]   U. Hansen, D. A. Yuen and S. E. Kroening,   Transition to hard turbulence in thermal convection at infinite Prandtl number,   Physics of Fluids A 2 (1990), 2157–2163.

[10]   T. J. R. Hughes, L. P. Franca and G. M. Hulbert,   A new finite element formulation for computational fluid dynamics: VIII. the galerkin/least-squares method for advective-diffusive equations,   Computer Methods in Applied Mechanics and Engineering 73 (1989) 173–189.

[11]   H. Itoh, M. Iga, K. Oda and H. Mase,   Mathematical model of unsteady molten glass flow with inhomogeneity in melt,   Proceedings of the XVII International Congress on Glass 6 (1995), 81–86, Chief Editor: Gong Fangtian.

[12]   H. Itoh, S. Yamamura, H. Todoriki and M. Iga,   Studies on flow structure in glass melting tank by mathematical model,   Proceedings of International Symposium on Glass problems 1 (1996), 408–414, Editor: Rena Akcakaya et al.

[13]   H. Itoh and M. Tabata,   A Finite Element Analysis for a Thermal Convection Problem at Infinite Prandtl Number,   to be published.

[14]   H. Jeffreys,   The stability of a layer of fluid heated below,   Philosophical Magazine and Journal of Science 7, 2 (1926), 833–844.

[15]   C. Johnson,   Numerical Solution of Partial Differential Equations by the Finite Element Method,   Cambridge University Press, Cambridge, 1987.

[16]   H. Kardestuncer,   Finite Element Handbook,   McGraw-Hill, 1987.

[17]   L. M. Luijkx, J. K. Platten,   On the onset of Free convection in a rectangular channel, Journal of Non-equilibrium Thermodynamics 6 (1981), 141–158.

[18]   H. Mase and K. Oda,   Mathematical model of glass tank furnace with batch melting process,   Journal of Non-crystalline Solids 38–39 (1980), 807–812.

[19]   D. P. McKenzie, J. M. Roberts and N. O. Weiss,   Convection in the earth's mantle: towards a numerical simulation,   Journal of Fluid Mechanics 62 (1974), 465–538.

[20]   L. Rayleigh,   On convection currents in a horizontal layer of fluid,   Philosophical Magazine and Journal of Science 6, 32 (1916), 529–546.

[21]   B. Reddy and H. Voye,   Finite element analysis of the stability of fluid motions,   Journal of Computational Physics 79 (1988), 92–112.

[22]   G. Schubert and C. A. Anderson,   Finite element calculations of very high Rayleigh number thermal convection,   Geophysical Journal for the Royal Astronomical Society 80 (1985), 575–601.

[23] M. Tabata and S. Fujima, An upwind finite element scheme for high-Reynolds number flows, International Journal for Numerical Methods in Fluids **12** (1991), 305–322.

[24] T. Tezduyar, M. Behr and J. Liou, A new strategy for finite element computations involving moving boundaries and interfaces—the deforming-spatial-domain/space-time procedure: I. the concept and the preliminary numerical tests, Computer Methods in Applied Mechanics and Engineering **94** (1992) 339–351.

[25] B. Travis and P. Olson, Convection with internal heat sources and thermal turbulence in the earth's mantle, Geophysical Journal International **118** (1994), 1–19.

[26] J. A. Whitehead and B. Parsons, Observations of convection at Rayleigh numbers up to 760,000 in a fluid with large Prandtl number, Geophysical and Astrophysical Fluid Dynamics **9** (1978), 201–217.

Asahi Glass Co. Ltd., Research Center,
1150, Hazawacho, Kanagawa-ku,
Yokohama 221-8755, Japan
and
Department of Mathematics,
Faculty of Science,
Hiroshima University,
Higashi-Hiroshima 739-8526, Japan